Contrib Mineral Petrol
DOI 10.1007/s00410-006-0143-y

ORIGINAL PAPER

Diffusion-controlled development of silica-undersaturated domains in felsic granulites of the Bohemian Massif (Variscan belt of Central Europe)

Lucie Tajčmanová · Jiří Konopásek · James A. D. Connolly

Received: 22 May 2006 / Accepted: 14 September 2006

Abstract Plagioclase rims around metastable kyanite crystals appear during decompression of high-pressure felsic granulites from the high-grade internal zone of the Bohemian Massif (Variscan belt of Central Europe). The development of the plagioclase corona is a manifestation of diffusion-driven transfer of CaO and Na_2O from the surrounding matrix and results in isolation of kyanite grains from the quartz- and K-feldspar-bearing matrix. This process establishes Si-undersaturated conditions along the plagioclase–kyanite interface, which allow crystallization of spinel during low-pressure metamorphism. The process of the plagioclase rim development is modeled thermodynamically assuming local equilibrium. The results combined with textural observations enable estimation of equilibration volume and diffusion length for Na and Ca that extends ~400–450 and ~450–550 μm, respectively, around each kyanite crystal. Low estimated bulk diffusion coefficients suggest that the diffusion rate of Ca and Na is controlled by low diffusivity of Al across the plagioclase rim.

Communicated by T.L. Grove.

L. Tajčmanová (✉) · J. Konopásek
Institute of Petrology and Structural Geology,
Charles University, Albertov 6,
128 43 Prague, Czech Republic
e-mail: kiki@natur.cuni.cz

L. Tajčmanová · J. Konopásek
Czech Geological Survey, Klárov 3,
118 21 Praha 1, Czech Republic

J. A. D. Connolly
Institut für Mineralogie und Petrographie,
ETH-Zentrum, 8092 Zürich, Switzerland

Keywords Equilibration volume · Coronal structures · Diffusion · Low-pressure granulites · Perple_X · Bohemian Massif

Introduction

Thermodynamic modeling of metamorphic processes is dependent on knowledge of the effective bulk composition of the system in question (Fisher and Elliott 1974). In the case of fluid-saturated rocks, the effective bulk composition is generally well approximated by the composition obtained by conventional whole-rock analysis. However, metamorphic reactions in water-deficient rocks, such as peridotites, eclogites, and granulites, are often limited by chemical diffusion (Mongkoltip and Ashworth 1983; Joesten 1991; Obata 1994; O'Brien 1999; Ashworth and Chambers 2000; Milke et al. 2001; Abart et al. 2004). In this case, the equilibration volume is small and the effective bulk composition must be estimated by other methods (Stüwe 1997).

The development of coronal textures at mineral interfaces has been studied extensively and is often described by diffusion models (Korzhinskii 1959; Brady 1977; Joesten 1977; Mongkoltip and Ashworth 1983; Ashworth and Birdi 1990; Ashworth 1993; Obata 1994; Ashworth and Chambers 2000; Milke and Heinrich 2002; Lang et al. 2004). These models describe development of layered coronas, where layer growth is accomplished by an exchange cycle of diffusion-controlled reactions in which components released by reaction at one contact of a layer diffuse through the layer to the opposite contact where they are consumed by another reaction and vice versa. In the steady state,

the stoichiometric coefficients of the reactions in the exchange cycle are controlled by the relative fluxes of the diffusing components within the growing layer. The fluxes, in turn, are controlled by the potential gradients within the layer and hence, are determined by the assemblage of the layer (Fisher 1973, 1978; Fisher and Elliott 1974). In models of this process, the phases in contact are usually treated as unlimited sources of elements participating in corona-producing reaction and coronal layers are explained by the different diffusivities of participating elements. Similar features are described in several studies on kyanite-bearing rocks in which plagioclase coronas separate metastable kyanite grains from matrix minerals that grew during decompression (Fig. 1) (Okay 1995; Nakamura and Hirajima 2000; Nakamura 2002; Möller 1998; O'Brien 1999). Although the resulting textures resemble those developed as a reaction product at the contact between two phases, the mechanism of plagioclase corona development is different because, at least in some rocks, the 'reacting' phases in mutual contact (e.g. kyanite and quartz) lack some of the elements necessary for plagioclase growth.

The development of plagioclase coronas requires diffusion of Na and Ca towards the metastable kyanite grain from a source region that may be recognized by a corresponding depletion in Na and Ca and the extent of this depletion defines the equilibration volume relevant to plagioclase corona development. Associated crystallization of Al-rich phases as spinel or corundum during the low-pressure re-equilibration of felsic high-pressure granulites or eclogite is common, but thermodynamically inconsistent with the presence of quartz as a matrix phase (O'Brien 1999; O'Brien and Rötzler 2003; Nakamura 2002; Dasgupta et al. 1995). Thus, the plagioclase coronas provide unambiguous evidence of disequilibrium and a mass transport controlled by diffusion, effects that complicate conventional thermobarometry. Here, following Korzhinskii (1959), we adopt a local equilibrium model to analyze plagioclase coronal textures (Fig. 1) developed in felsic granulites of the Bohemian Massif in order to constrain the thermobarometric conditions of their low-pressure reequilibration and quantify the associated equilibration volume. Material re-distribution during coronal growth occurred with little contribution by fluid (or melt) movement (Tajčmanová et al. 2006) and thus we assume that nearly solid-state diffusion processes played a major role during the transition from high- to low-pressure stage.

Sample description

The studied samples are felsic granulites from the high-grade eastern margin of the Moldanubian domain of the Bohemian massif (Variscan belt of Central Europe) (Fig. 2). Metamorphic evolution of the studied granulite and surrounding rocks has been described in Tajčmanová et al. (2006). The early high pressure (HP) mineral assemblage is represented by Grt–Ky–Pl–Kfs–

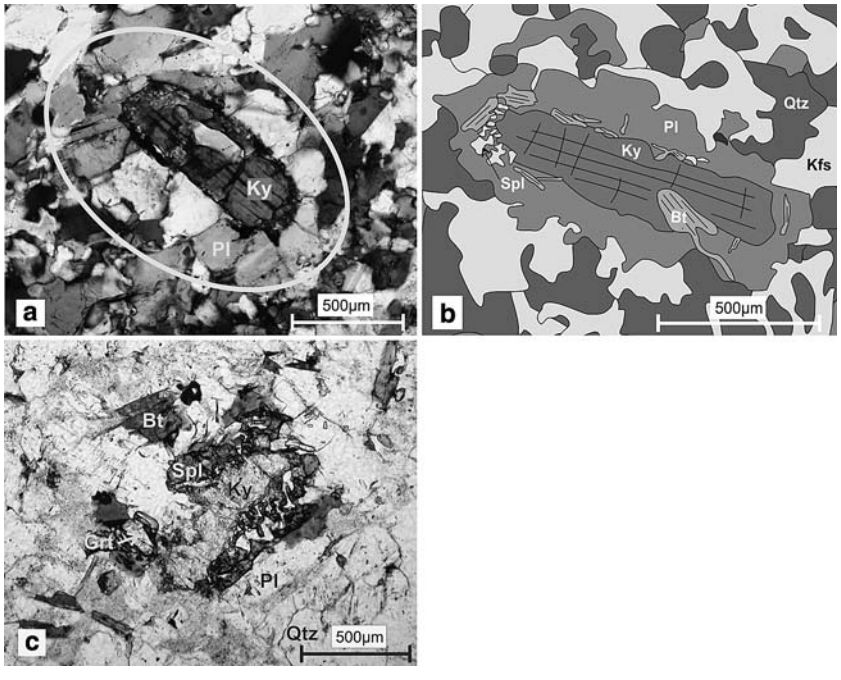

Fig. 1 **a** Photomicrograph and **b** schematic figure of studied Al-rich domain represented by metastable kyanite grain surrounded by plagioclase rim. **c** Photomicrograph of low-pressure mineral assemblage Ky–Bt–Spl–Pl-matrix (Qtz + Kfs) in studied samples of felsic granulite

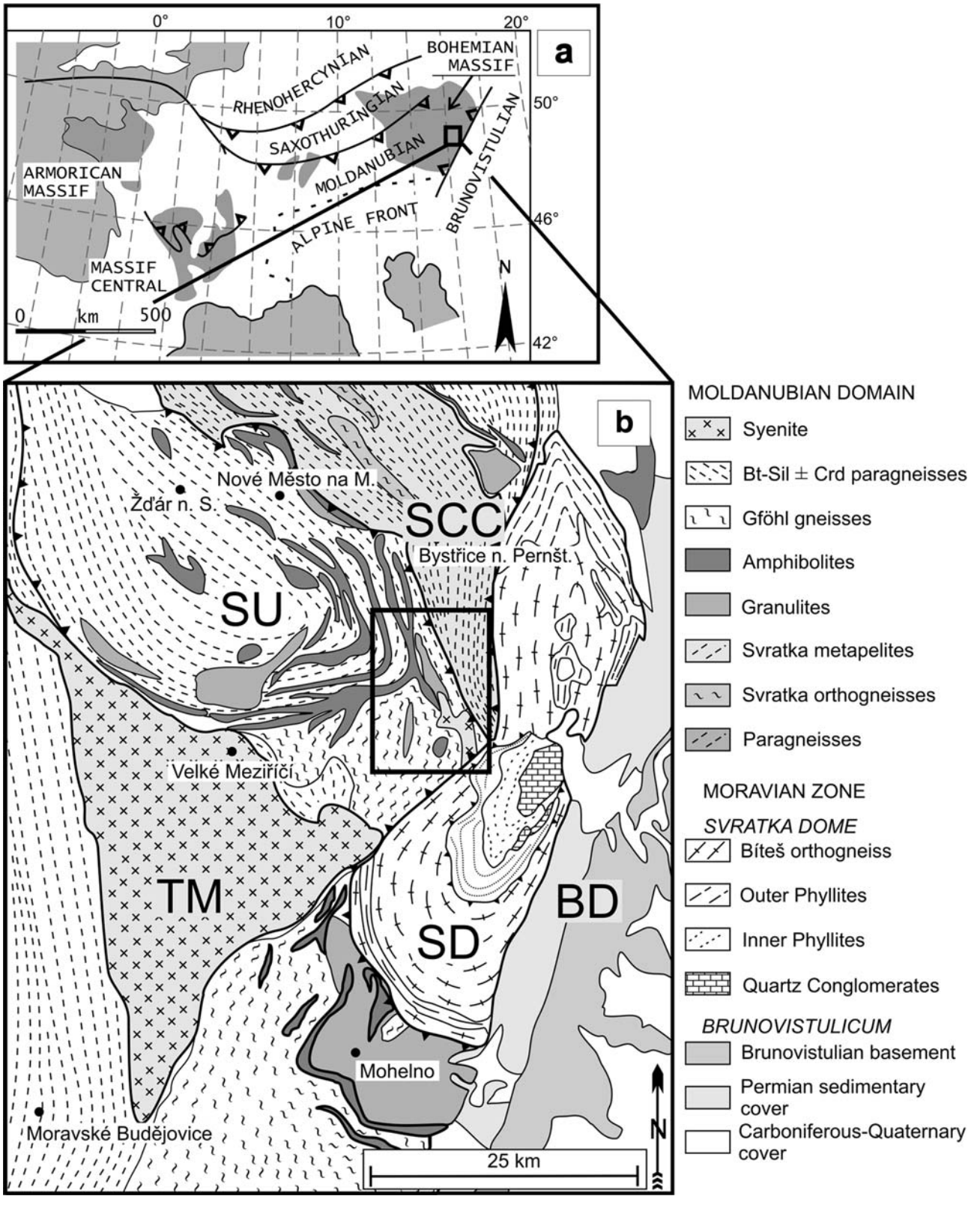

Fig. 2 **a** The location of the study area in the European Variscides (*solid square* in the eastern part of the Bohemian Massif). **b** Geological map of the north-eastern part of the Moldanubian zone (Bohemian Massif). The *solid square* represents the area of interest. *TM* Třebíč massif, *SU* Strážek unit-orogenic lower crust, *SCC* Svratka complex-middle crust, *SD* Svratka dome, *BD* Brunovistulian domain

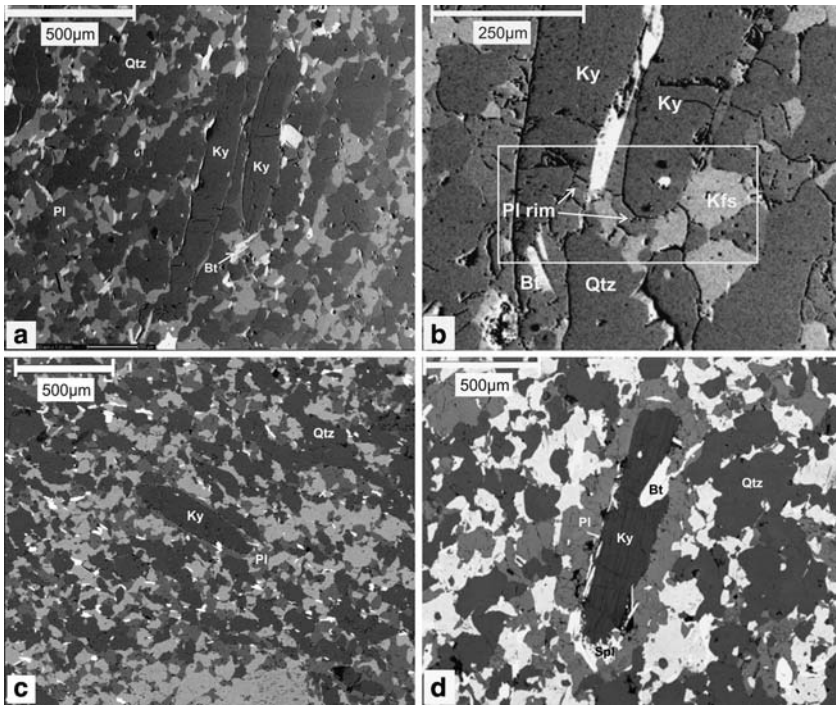

Fig. 3 **a** Back-scattered electron (BSE) image of textural relationships in high-pressure granulite sample. Kyanite is in direct contact with quartz and K-feldspar and matrix is composed of randomly ordered small plagioclase, quartz and K-feldspar grains. **b** BSE image showing an early development of the plagioclase rim. Plagioclase grows preferentially along the kyanite–quartz interface, whereas the K-feldspar–kyanite interface remains largely stable. The early crystals of biotite are already enclosed in the rim. **c** BSE image of high-pressure granulite sample with paragenetically early thin plagioclase rim around kyanite. **d** BSE image of low-pressure granulite sample in which kyanite is never in contact with quartz

Qtz–(Liq) which equilibrated at ~850°C and 18 kbar. The presence of melt is presumed given the metamorphic conditions estimated for the HP stage, which are beyond the stability of muscovite + quartz (Tajčmanová et al. 2006). The absence of evident melt segregations is explicable given that the amount of melt computed by thermodynamic modeling (White et al. 2001) is low (<5%). Kyanite is commonly replaced by sillimanite and garnet is partially consumed by biotite suggesting the stabilization of the low pressure (LP) assemblage Grt–Sil–Bt–Pl–Kfs–Qtz–(Liq). In samples with LP overprint, coronal structures formed as a result of decompression. These structures are characterized by a rim of plagioclase that isolates metastable kyanite grains from the matrix (Fig. 1a, b). The degree of development of such coronas is variable in samples representing different evolution stages. The coronal structures are randomly distributed and represent about 10% of the rock volume. The aggregates of metastable kyanite crystals with plagioclase rim are quartz free and contain spinel-bearing mineral assemblages typical of low pressure/high temperature (LP/HT) metamorphism (Fig. 1b, c).

Coronal structure development

In typical HP samples (Fig. 3a), kyanite is in direct contact with quartz and K-feldspar and the matrix is composed of randomly oriented small plagioclase ($An_{14–16}$), quartz and K-feldspar grains. Garnets are randomly distributed in the rock with no particular affinity with the kyanite-bearing domains. In several HP samples, paragenetically early thin plagioclase coronas rim kyanite grains. In these samples it is possible to observe how both reactants quartz and kyanite produce the plagioclase rim (Fig. 3b, c). The crystallization of plagioclase between K-feldspar and kyanite is not observed in these early stages of decompression and is probably connected with advanced stages of the plagioclase rim development.

In LP samples, kyanite grains are never in contact with quartz (Fig. 3d). Plagioclase rims isolate kyanite crystals from the matrix and consist of grains of ~0.06 mm in diameter. The shape of the coronal structure is controlled by the former shape of the kyanite grain. The plagioclase rims have a radial thickness of 200–250 μm and show chemical zoning

Table 1 Representative electron microprobe analyses of feldspars from the high- and low-pressure samples of felsic granulite

	High-pressure stage			Low-pressure stage		
	Pl mt	Pl ky	Kfs mt	Pl 1	Pl 2	Kfs mt
wt%						
SiO_2	65.28	64.28	64.48	62.01	63.80	64.41
TiO_2	0.00	0.00	0.00	0.00	0.00	0.05
Cr_2O_3	0.00	0.00	0.00	0.00	0.00	0.00
Al_2O_3	21.95	22.41	18.24	23.48	22.50	18.89
FeO	0.00	0.00	0.04	0.03	0.03	0.04
MnO	0.00	0.00	0.00	0.00	0.08	0.09
MgO	0.00	0.00	0.00	0.00	0.00	0.01
ZnO	0.00	0.00	0.00	0.00	0.00	0.00
CaO	3.16	3.35	0.03	4.83	3.64	0.02
Na_2O	9.86	9.79	1.31	8.95	9.74	1.62
K_2O	0.28	0.22	15.21	0.13	0.17	14.69
F	0.00	0.00	0.00	0.00	0.00	0.00
Cl	0.00	0.00	0.00	0.00	0.00	0.00
Total	100.52	100.05	99.31	99.415	99.96	99.82
XAn	0.15	0.16	0.00	0.23	0.17	0.00
XAb	0.84	0.83	0.12	0.765	0.82	0.14
XOr	0.02	0.01	0.88	0.01	0.01	0.86

Pl mt plagioclase in matrix, *Pl ky* plagioclase of the early plagioclase rim, *Pl 1* plagioclase close to kyanite, *Pl 2* plagioclase close to matrix

with compositions ranging from An_{22} at the kyanite side to An_{16} near the quartz side (Table 1). This 'compositional gradient' is represented by an Al-rich/Si-poor and a Si-rich/Al-poor layer in plagioclase that masks the primary contact between kyanite and quartz. The former quartz is completely or partly consumed.

To visualize the effect of the plagioclase rim development, backscatter electron images (BSE) for all stages of the plagioclase rim development were obtained and used for image analysis of the area around kyanite grains. The image analysis method was completed with Lucia G 5.00 software. Results (Fig. 4a) show randomly distributed fine-grained plagioclase in the matrix around kyanite in the high-pressure stage, whereas strong depletion of plagioclase in the immediate vicinity of the kyanite crystal in the matrix and its concentration around kyanite is observed for the low-pressure stage (Fig. 4b).

Sample mineralogy

High-pressure stage

Composition of the mineral phases stable in the HP stage has been described by Tajčmanová et al. (2006). Biotite is in contact with kyanite in the early stages of coronal structure development (Fig. 3a, b) and appears at the expense of garnet still in the kyanite stability field (Tajčmanová et al. 2006). The zinc content of high-pressure garnets is ~200 ppm, whereas that of biotite is ~600 ppm suggesting strong partitioning of this element into newly grown biotite.

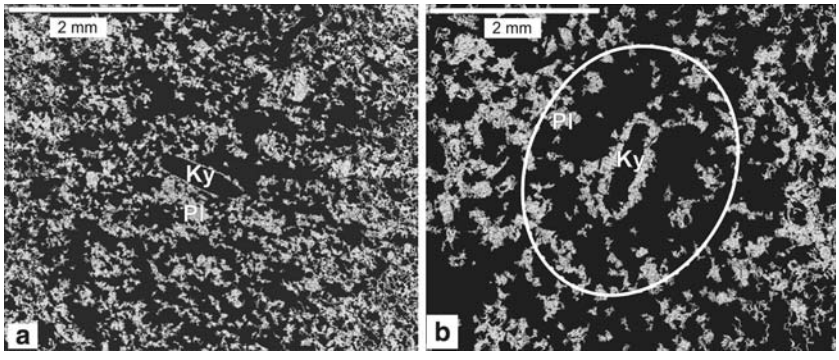

Fig. 4 Results of the image analysis of BSE images performed using the Lucia G 5.00 software. After processing, plagioclase is shown in *white*, whereas all other phases are shown in *black*. **a** Randomly distributed fine-grained plagioclase in the matrix around kyanite in the high-pressure granulite sample. **b** Depletion of plagioclase in the immediate vicinity of the kyanite crystal in the matrix and its concentration around kyanite in the low-pressure granulite sample

Low-pressure stage—coronal structures

Coronal structures in studied samples have the mineralogy Ky–Pl–Bt–Sp ± Grt–(Liq). *Biotite* shows no compositional zoning and commonly contains 0.11–0.20 p.f.u Ti and ~50–100 ppm Zn. The X_{Mg} (Mg/(Mg + Fe^{2+})) value is 0.30 and inferred tetrahedral Al contents range from 1.3 to 1.4 p.f.u. *Spinel* is present exclusively within the coronal structure and crystallizes between previously enclosed biotite and relics of kyanite grains. Spinel corresponds to spinel–hercynite–gahnite solid solution with moderate zinc contents (0.05–0.09 Zn p.f.u) and X_{Mg} in the range from 0.05 to 0.10.

Low-pressure stage—depletion haloes

The area around coronal structures shows significant depletion in plagioclase and its mineralogy is Kf–Qtz–Bt ± Plg ± Grt. *Biotite* has the same composition as that enclosed in coronal structures. *Garnet* is essentially an almandine–pyrope solid solution with only minor grossular component. Most garnet grains are chemically homogeneous with only slightly decreasing X_{Mg} towards the rims ($X_{Mg0.10 \rightarrow 0.07}$); other components remain relatively constant (Grs_0; $Prp_{10 \rightarrow 7}$; $Alm_{84 \rightarrow 88}$; $Sps_{3 \rightarrow 4}$). The absence of chemical zoning and the low-Ca content in most of the garnets suggest complete re-equilibration during the transition from high- to the low-pressure stage. Composition of *plagioclase* is the same as the composition of outer parts of the plagioclase corona. *K-feldspar* contains up to 16 mol% of albite and no significant anorthite component.

Representative microprobe analyses of minerals and formula units to which the mineral is recalculated are listed in Tables 1 and 2. The analyses of major elements were carried out on a Cam-Scan S4 with Link ISIS 300 EDX analyzer at Charles University in Prague and on a CAMECA SX100 at Masaryk University in Brno. Operating conditions were 15 kV accelerating voltage, 0.56 nA beam current, 120 s acquisition lifetime on Cam-Scan and 15 kV accelerating voltage, 10–20 nA beam current, acquisition lifetime ranging from 10 to 30 s on CAMECA. Mineral abbreviations are after Kretz (1983). Zinc content in biotite and garnet was measured by laser ablation ICP-MS at the University of Bergen.

Material transfer

Microstructural relationships in the above-described LP granulites indicate that the plagioclase coronas between quartz and metastable kyanite form by the reaction:

$$Ky + Qtz + Na_2O + CaO = Pl \quad (1)$$

where Na_2O and CaO are presumed to be supplied by diffusion from the former matrix plagioclase during decompression.

As plagioclase is the only phase containing the Na_2O component in the rock the availability of former plagioclase in the matrix controls the development of the later plagioclase domain. The boundaries among matrix grains and concentric plagioclase coronas around kyanite are sharp. Unfortunately, the minor changes in chemical composition of participating phases over the domain and in its surrounding do not allow quantification of the component mobility.

Pressure–temperature estimates and problem of equilibration volume

To constrain the pressure–temperature (*P–T*) conditions of the low-pressure re-equilibration, *P–T* phase diagram sections were computed for the bulk rock composition (Fig. 5a) and a composition estimated from the chemistry and amounts of the constituent phases (Fig. 1b), chosen to represent the coronal structure (Fig. 5b). All calculations reported here were made with the thermodynamic database of Holland and Powell (1998, revised 2002) and the Perple_X computer program (Connolly 2005). Mixing properties of phases used for the calculation were taken from Berman (1990) for garnet, Newton et al. (1980) for plagioclase, Thompson and Hovis (1979) for K-feldspar, Nichols et al. (1992) for spinel, Powell and Holland (1999) for biotite and cordierite, and White et al. (2001) for melt. The resulting *P–T* section for the bulk rock composition (Na_2O = 2.58, CaO = 1.90, K_2O = 2.71, FeO = 4.20, MgO = 2.57, Al_2O_3 = 13.52, SiO_2 = 71.73, H_2O = 0.80, molar amounts) does not have a stability field for spinel (Fig. 5a), which demonstrates that the whole rock composition is inappropriate for thermobarometric analysis of the LP assemblage. In contrast, the *P–T* section computed for the composition of the coronal structure (Na_2O = 5.51, CaO = 3.38, K_2O = 0.46, FeO = 6.94, MgO = 1.37, Al_2O_3 = 26.32, SiO_2 = 55.21, H_2O = 0.81, molar amounts) shows a quartz-absent quadrivariant stability field for the assemblage Grt–Sil-Bt-Pl-Spl-(Liq) (Fig. 5b). The chemical composition of the particular phases from the assemblage is fully consistent with the observed mineral assemblages within the plagioclase–

Table 2 Representative electron microprobe analyses of Fe–Mg phases from high- and low-pressure samples of the granulite

	High-pressure stage			Low-pressure stage			
	Bt	Grt1 core	Grt1 rim	Bt	Spl	Grt core	Grt rim
wt%							
SiO_2	36.90	38.83	37.34	34.75	0.02	36.68	36.18
TiO_2	4.65	0.00	0.00	3.52	0.00	0.07	0.05
Cr_2O_3	0.00	0.00	0.00	0.00	0.00	0.00	0.00
Al_2O_3	18.39	21.80	21.75	19.83	58.27	20.63	20.21
FeO	15.48	25.83	28.30	22.78	35.54	38.38	39.22
MnO	0.00	0.58	0.98	0.00	0.37	1.69	1.54
MgO	11.57	7.12	5.45	5.85	2.39	2.35	1.80
ZnO	0.00	0.00	0.00	0.00	2.80	0.00	0.00
CaO	0.00	5.95	5.39	0.00	0.00	0.62	0.52
Na_2O	0.00	0.00	0.00	0.00	0.00	0.00	0.00
K_2O	9.79	0.00	0.00	10.06	0.00	0.00	0.00
F	0.00	0.00	0.00	0.00	0.00	0.00	0.00
Cl	0.00	0.00	0.00	0.00	0.00	0.00	0.00
Total	96.78	100.11	99.21	96.79	99.38	100.43	99.52
XMg	0.57	0.33	0.26	0.31	0.10	0.10	0.08
XGrs	–	0.16	0.12	–	–	0.02	0.00
XAlm	–	0.55	0.61	–	–	0.85	0.87
XPrp	–	0.27	0.22	–	–	0.10	0.07
XSps	–	0.01	0.02	–	–	0.04	0.04

kyanite domains typical of LP re-equilibration in the felsic granulites and suggests their equilibration at 710–740°C and 4.5–6 kbar. This estimate matches that for the surrounding cordierite-bearing gneisses made by Tajčmanová et al. (2006).

Compositional *X–X* sections

The development of the decompression coronal structure is related to the presence of metastable kyanite grains, which are randomly distributed in the rock. The

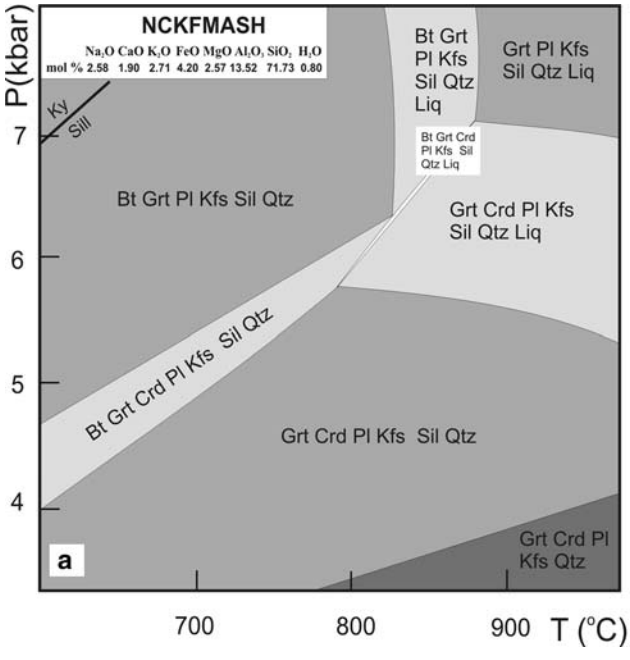

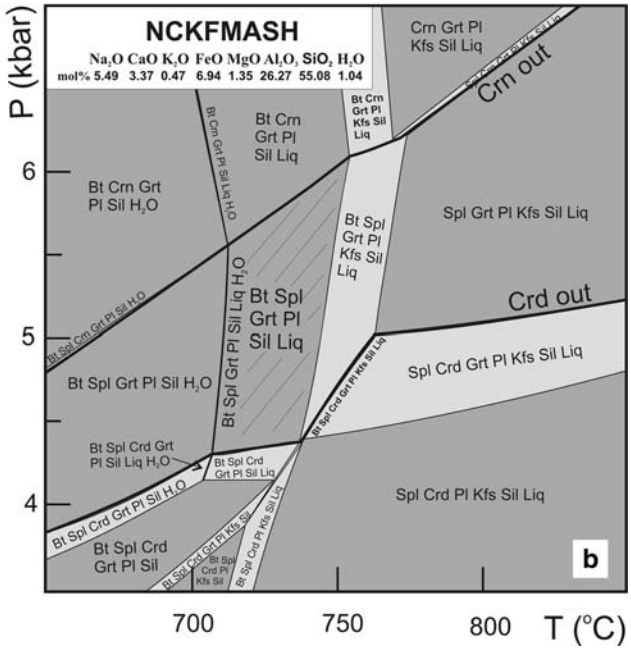

Fig. 5 **a** *P–T* section for low-pressure stage in felsic granulites calculated in NCKFMASH system. System composition (in mol%) used for calculation is presented in *upper left inset* and corresponds to the whole rock analysis. **b** *P–T* section for low-pressure stage in felsic granulite calculated in NCKFMASH system. System composition (in mol%) used for calculation is presented in *upper left inset* and corresponds to the effective molar bulk composition of the local domain around metastable kyanite

kyanite grains and their immediate surrounding create local aluminum-rich domains. These domains comprise ~10% of the whole rock volume and thus they do not significantly influence the bulk composition. To understand the variability in chemical composition within the rock at certain pressure–temperature conditions, phase relations were computed as a function of the stoichiometric components: C_0, the bulk composition in the immediate vicinity of the kyanite grain (Fig. 3a), C_1 = (0.71 MgO + 3.60 FeO), and C_2 = (2.67 Na_2O + 1.64 CaO) chosen to represent the major compositional variations during the formation of the low-pressure domains. In the resulting *X*-*X* section (Fig. 6) the composition at any point is $C = C_0 + X_1C_1 + X_2C_2$, where X_1 and X_2 vary between zero and one along the horizontal and vertical axes, respectively. In the *X*-*X* section, the spinel-bearing assemblage (Figs. 1c, 3d) corresponding to that of the *P*–*T* section (Fig. 5b) is stable beyond the curve representing quartz-saturated compositions. An overstepping of this curve is related to continuously increasing amount of Na_2O and CaO components added to the starting composition, which corresponds to the development of plagioclase rim enveloping metastable kyanite grains in the granulite sample. The plagioclase rim defines the boundary of the quartz-free domain and the development of this domain due to increasing amount of crystallized plagioclase is documented by modal isopleths of plagioclase and quartz (Fig. 6).

The *P*–*T* section for the composition of the coronal structure (Fig. 5b) shows that the observed mineral association with spinel can only develop at quartz-undersaturated conditions (quartz-absent stability field). This observation is confirmed by the phase relations in the *X*–*X* section that show a transition

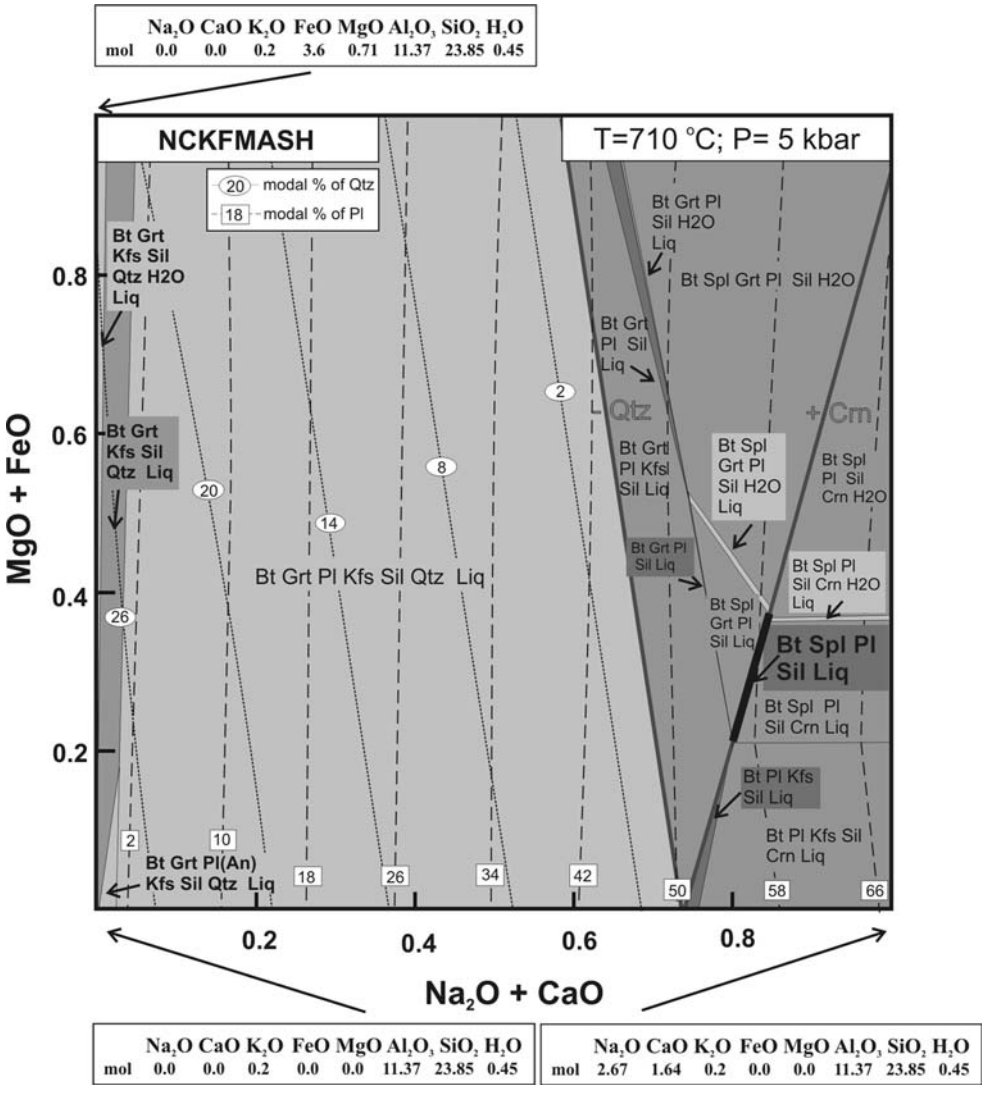

Fig. 6 *X*–*X* section at 710°C and 5 kbar. The stability field with the assemblage Bt–Spl–Sil–Pl–(Liq) corresponds to the *narrow black field* in the *lower right corner* of the diagram. Towards the spinel stability field, modal amount of quartz decreases as the amount of plagioclase increases

Table 3 Illustration of the strategy adopted for calculation of an equilibration volume for Na_2O and CaO necessary for the plagioclase rim development. Molar values were taken from the werami.exe routine of the Perple_X software set

PL CORONA	mol	Molar fraction	Molar volume of the system (mm^3/mol)	x_i per mm^3 (mol/mm^3)	V^{Plrim} (mm^3)	$V^{Plrim} * x_i^{rim}$ (mol/V_{Plrim})
CaO	2.35	0.056	1.05E + 06	5.28E-08	0.0586	3.10E-09
Na_2O	3.82	0.091	1.05E + 06	8.61E-08	0.0586	5.05E-09
Sum of mols in the system	41.43	–	–	–	–	–
MATRIX	mol	Molar fraction	Molar volume of the system (mm^3/mol)	x_i per mm^3 (mol/mm^3)	V^{matrix} (Eq. 2) (mm^3)	Radius (L_d) (Eq. 5) (mm)
CaO	1.00	0.010	2.32E + 06	4.47E-09	0.693	0.547
Na_2O	2.99	0.031	2.32E + 06	1.33E-08	0.378	0.416
Sum of mols in the system	96.63	–	–	–	–	–

from the HP mineral assemblage Ky–Qtz–Kfs ± Bt–(Liq) (Fig. 3a) to quartz-free/Al-rich mineral assemblages involving spinel or corundum as observed within the coronal structures (Figs. 1c, 3d).

Equilibration volume derivation—calculation technique

Because the coronal structures develop between quartz and kyanite, a minimal model for their formation must allow for the diffusion of Na_2O and CaO. To construct a first-order estimate of the equilibration volume relevant for plagioclase rim growth we assume that only Na_2O and CaO were mobile and neglect the small volume effects associated with rim growth. The plagioclase composition is used as an estimate for the bulk composition of the reactive portion of the coronal structure and the whole rock composition is used as an estimate of the matrix composition. The volume (V) of matrix that would be depleted in either component is then

$$V^{\text{matrix}} = V^{\text{rim}} x_i^{\text{rim}} / \Delta x_i^{\text{matrix}} \tag{2}$$

where x_i^{rim} is the concentration in moles per unit volume of the component in the rim and $\Delta x_i^{\text{matrix}}$ is the change in the concentration of the component in the depletion halo (Table 3). For spherical geometry (Fig. 7), the volumes of the plagioclase rim and matrix are

$$V^{\text{matrix}} = \frac{4}{3}\pi((r_0 + L_{\text{d}})^3 - r_0^3) \tag{3}$$

$$V^{\text{rim}} = \frac{4}{3}\pi((r_0 + L_{\text{rim}})^3 - r_0^3) \tag{4}$$

where r_0 is the radius of the metastable kyanite grain, and L_{rim} and L_{d} are, respectively, the widths of the plagioclase rim and the depletion halo. Substituting Eqs. 3 and 4 into Eq. 2 and solving for L_{d} yields an estimate for the diffusion length scale

$$L_{\text{d}} = \sqrt[3]{r_0^3 + x_i^{\text{rim}} L_{\text{rim}} \frac{(3r_0(r_0 + L_{\text{rim}}) + L_{\text{rim}}^2)}{\Delta x_i^{\text{matrix}}}} - r_0 \tag{5}$$

The kyanite grains are sometimes better approximated as ellipsoids than spheres, but in view of the small resulting correction to the equilibration length (<3%) use of the less cumbersome spherical model is justified here.

The results indicate an equilibration volume for Na that extends ~400–450 μm and for Ca that extends ~450–550 μm around each kyanite (Table 3). This is

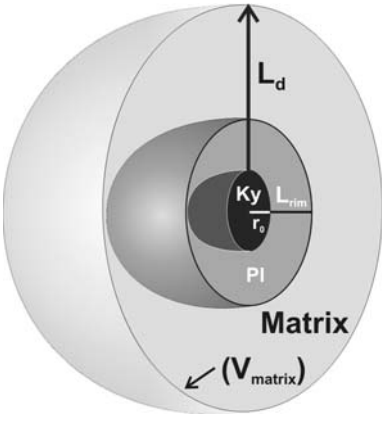

Fig. 7 Schematic figure of different layers forming the local Al-rich domain and its surrounding used for calculation of equilibration volume necessary for the plagioclase rim development

in agreement with result from image analysis that shows significant depletion of the matrix in plagioclase around kyanite crystal on this spatial scale (Fig. 4b).

Discussion

The role of equilibration volume and diffusion mass transfer

Our analysis of plagioclase coronas developed around metastable kyanite grains confirms that modeling of metamorphic reactions in high-grade rocks requires careful estimate of equilibration volume because of the limited scale of equilibration at fluid-deficient conditions. Under nearly dry conditions, diffusion controlled mineral reactions are the result of local gradients in chemical potential (Fisher 1973, 1978; Nakamura 2002), which drive diffusion mass transfer due to disequilibrium in the system as a whole.

The development of plagioclase coronas around kyanite in granulites of this study is the result of the stabilization of increasingly anorthite-rich plagioclase during decompression. The Al_2O_3 and SiO_2 necessary for the growth of the coronas are presumably derived largely from the original kyanite–quartz interface, whereas CaO and Na_2O must be supplied by diffusion from the matrix plagioclase. CaO and Na_2O components are transferred towards the kyanite–quartz interface, whereas Al and Si cations from former plagioclase stay in situ due to their lower mobility and participate in crystallization of newly grown quartz and biotite in the depletion haloes (Fig. 8). This model is confirmed by the presence of biotite-bearing depletion haloes (Fig. 4b) in the matrix around the plagioclase coronas. The size of the depletion halo also permits quantification of the equilibration length and volume relevant for the growth process.

The progressive isolation of kyanite from the quartz-rich matrix due to the development of plagioclase rim can be modeled by adding CaO + Na_2O components to the composition corresponding to the immediate vicinity of the kyanite grain (Fig. 6). This process leads to continuous increase in modal amount of plagioclase at the expense of quartz and kyanite, and results in establishment of SiO_2-undersaturated and Al-rich environment inside the plagioclase rim. The presence of kyanite together with enclosed biotites in the quartz-free domain leads to the crystallization of spinel at low-pressure conditions, and equilibration volume necessary for the stabilization of spinel is thus restricted to the interior of the plagioclase domain.

The variation in the stable mineralogy during decompression can be monitored by changing of the bulk composition in a *P–X* diagram (Fig. 9). In this diagram the bulk composition variability represents a transition from matrix composition (whole rock composition) at point 0 towards Al-rich composition calculated from immediate kyanite surrounding (point 1) on the *X*-axis. The diagram shows that cordierite can be stable in an assemblage with quartz, whereas corundum and spinel require a SiO_2-undersaturated environment. Which of these two phases will be stable is the function of pressure conditions under which the quartz-out line is overstepped at given temperature.

The above-derived technique for equilibration volume estimates cannot be used for the FeO and MgO components, as there is no prominent effect of their diffusion on the rock texture. The reason is the high diffusivity of these components (Keller et al. 2006) allowing their high mobility and resulting in apparently uniform distribution of biotite throughout the whole volume of the rock. Regarding higher zinc content in the HP biotites and strong depletion of zinc in the biotite from the LP coronas we assume that observed zinc-rich spinels crystallize at the expense of former biotite. In samples where no biotite is enclosed in the plagioclase rim, spinel does not crystallize.

The presence of melt, in general, may increase the efficiency of redistribution of all cations over the given equilibration volume of the matrix. We suppose that up to 1–5% of melt might have been present in studied samples regarding the HP/HT dry conditions of the rock (Tajčmanová et al. 2006), which is in good

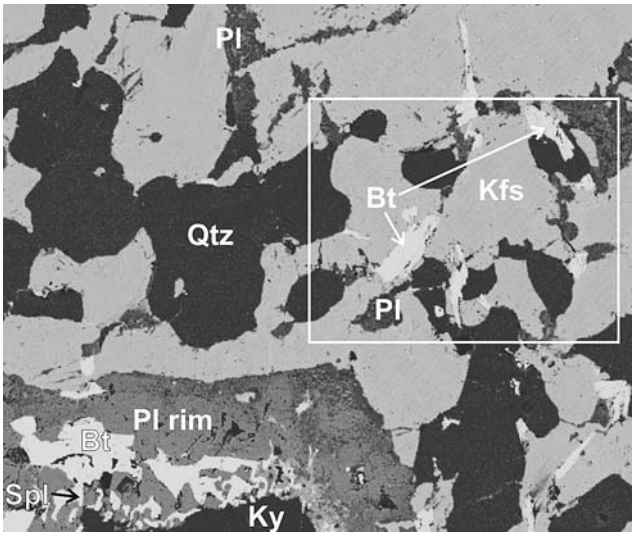

Fig. 8 Photomicrograph showing part of the depletion halo with relics of early plagioclase, newly grown biotite and quartz

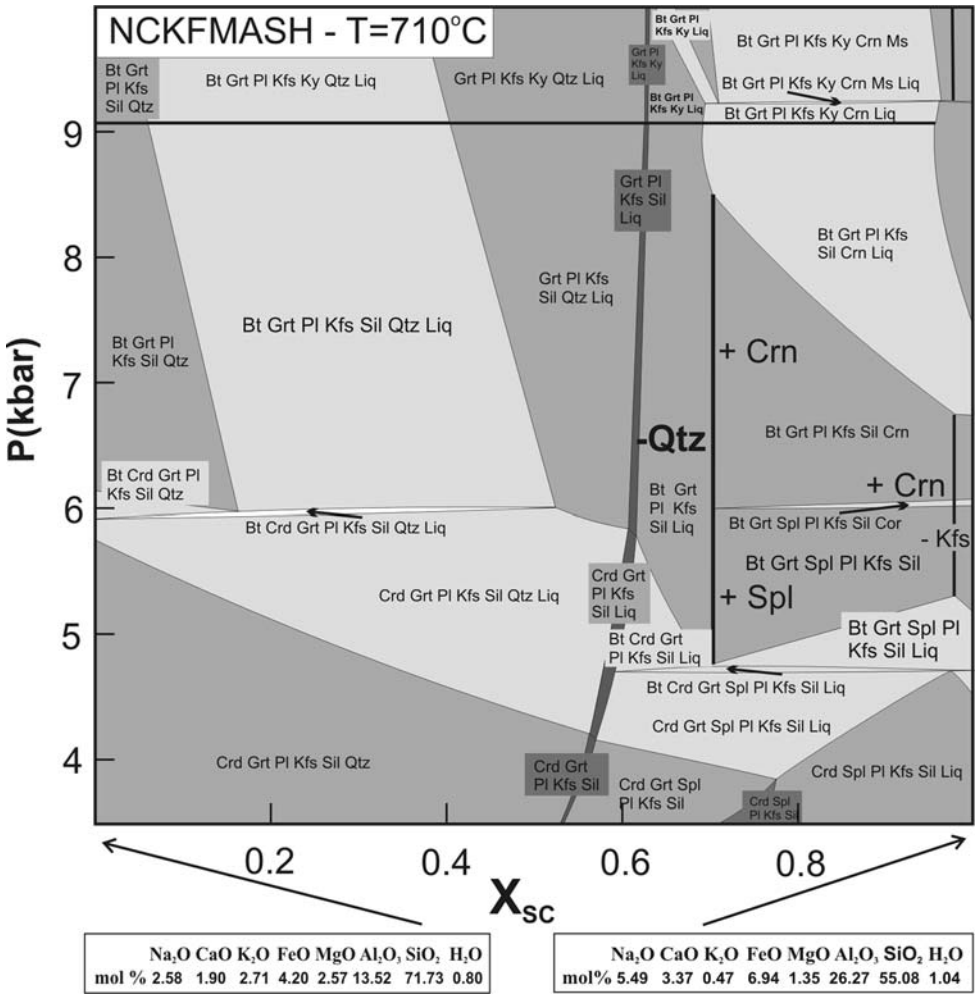

Fig. 9 *P–X* section calculated for the whole rock composition of the felsic granulite sample at point 0 and the composition of the immediate surrounding of the kyanite grain at point 1 on the *X*-axis. The diagram shows that the crystallization of spinel or corundum requires the quartz-undersaturated environment

agreement with lack of macroscopic melt segregations in studied samples. Low calculated diffusivities (see below) suggest that such low amount of melt did not effectively increase cation mobility.

Diffusion coefficients and rate-controlling species

This work presumes that the rate-limiting process controlling the growth of the coronal structures is the diffusion of Na_2O and CaO from the decomposing matrix plagioclase grains. Alternatively, it might be postulated that the kinetics of plagioclase decomposition is the rate-limiting process. We favor the model in which diffusion is rate limiting because the decomposition is spatially associated with the coronal structures, suggesting a transport controlled process.

In our samples the volume of a rock affected by LP re-equilibration is a function of effective diffusivity (D) of a certain element and time (t) available for the diffusion-driven changes at given temperature. In polycrystalline material such as quartz–feldspar matrix, diffusion processes include volume (through grain interiors) and grain- or interphase-boundary diffusions (Joesten 1991; Kaur et al. 1995). We cannot infer which of these mechanisms control the movement of the diffusing components and we thus deal only with bulk diffusion and effective diffusion coefficients (Brady 1983).

If the time of growth of the plagioclase rim is known (e.g. from available geochronological data), we can calculate an effective diffusivity (D) of a given component at given temperature. From calculated equilibration volume we can estimate the diffusion length L_d. As a time value (t) in the general equation for diffusion in a sphere

$$L_d = \sqrt{4Dt}, \quad (6)$$

it is possible to use available geochronological data for HP and LP stages in the studied samples (Schulmann et al. 2005) and apply them to calculate the effective diffusivity of Na_2O and CaO components. Geochronological data yield the maximum time interval of transition from HP to LP stage to be ~17 Ma indicating the growth rates of plagioclase rim of about 0.012–0.014 mm/Ma. With observed and calculated diffusion length of ~400–550 μm, resulting effective diffusion coefficients calculated with Eq. 6 are ~10^{-22}–10^{-23} m^2/s. There are uncertainties in estimates of duration of the growth process, but as we observe early stages of the plagioclase rim developed already during the high-pressure stage (Fig. 3b, c), the minimum time difference of 9 Ma between the high- and low-pressure metamorphism taken from geochronological data (Schulmann et al. 2005) would imply only slightly higher effective diffusivities for observed diffusion length. Small differences in diffusion lengths of CaO and Na_2O components (around 100 μm) indicate similar relative mobilities of these components under nearly solid-state conditions observed in studied samples.

The experimental data of Farver and Yund (1995) for Ca in plagioclase (at 700–1,100°C) and of Brady and Yund (1983) and Christoffersen et al. (1983) for K–Na in albite to intermediate plagioclase (at 600°C) show diffusivities in range of ~10^{-20} and ~10^{-18} m^2/s, respectively. If the process of the plagioclase rim development took place with Ca and Na diffusivities of this magnitude, then the equilibration length scale would be approximately three times higher than observed for the time scale indicated by geochronology (Fig. 10). To reconcile this discrepancy a time scale of < 1 My would be required, which seems implausible in view of the estimated error for the geochronology. An explanation for the discrepancy between the experimental and field based Ca and Na diffusivities is that the transport rates of these components, and consequently the thickness of the plagioclase rim, are controlled by low diffusivities of Al_2O_3 and/or SiO_2 (Mongkoltip and Ashworth 1983). Resulting diffusion coefficients for CaO and Na_2O components calculated from our samples are thus effective values that are influenced by the availability of Al_2O_3 and SiO_2 in the vicinity of kyanite crystal to form new plagioclase. Our natural example also demonstrates possible pitfall connected with application of experimentally determined diffusivities without careful assessment of all textural changes occurring in the rock.

Acknowledgements This work was financially supported by Charles University Grant Agency (GAUK no. 333/2004/B-GEO/PrF) and by Project of the Czech Geological Survey and Ministry of Environment (No. 6352). We gratefully acknowledge R. Čopjaková, R.Škoda from Masaryk University in Brno and R. Procházka from Charles University in Prague for operating the microprobe. J. Košler is acknowledged for the ICP-MS measurements. Two anonymous reviewers are thanked for their constructive reviews and T. L. Grove is gratefully thanked for his careful editorial work.

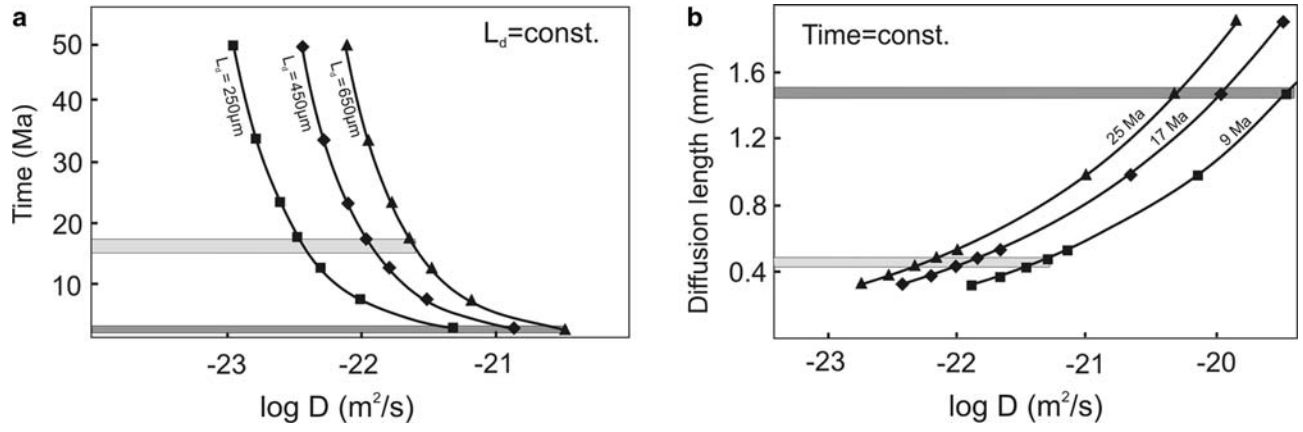

Fig. 10 The diagrams showing the variability of the diffusion coefficient for CaO with **a** time at given diffusion length and with **b** diffusion length at given time span. In both diagrams, the values calculated for diffusion coefficient estimated in this work are shown in *light gray*, whereas the values calculated with diffusion coefficients experimentally determined by Farver and Yund (1995), Brady and Yund (1983) and Christoffersen et al. (1983) are shown in *dark gray*. Results from this work suggest diffusion coefficients, which are approximately two orders of magnitude lower than those estimated by the above-mentioned authors

References

Abart R, Kunze K, Milke R, Sperb R, Heinrich W (2004) Silicon and oxygen self diffusion in enstatite polycrystals: the Milke et al. (2001) rim growth experiments revisited. Contrib Mineral Petrol 147(6):633–646

Ashworth JR (1993) Fluid-absent diffusion kinetics of Al inferred from retrograde metamorphic coronas. Am Mineral 78:331–337

Ashworth JR, Birdi JJ (1990) Diffusion modelling of coronas around olivine in an open system. Geochim Cosmochim Acta 54:2389–2401

Ashworth JR, Chambers AD (2000) Symplectic reaction in olivine and the controls of intergrowth spacing in symplectites. J Petrol 41(2):285–304

Berman RG (1990) Mixing properties of Ca–Mg–Fe–Mn garnets. Am Mineral 75:328–344

Brady JB (1977) Metasomatic zones in metamorphic rocks. Geochim Cosmochim Acta 41:113–125

Brady JB (1983) Intergranular diffusion in metamorphic rocks. Am J Sci 283A:181–200

Brady JB, Yund RA (1983) Interdiffusion of K and Na in alkali feldspar: homogenization experiments. Am Mineral 68:106–111

Christoffersen R, Yund RA, Tullis J (1983) Inter-diffusion of K and Na in alkali feldspars: diffusion couple experiments. Am Mineral 68:1126–1133

Connolly JAD (2005) Computation of phase equilibria by linear programming: a tool for geodynamic modeling and its application to subduction zone decarbonation. Earth Planet Sci Lett 236(1–2):524–541

Dasgupta S, Sengupta P, Juergen E, Raith M, Bardhan S (1995) Reaction textures in a suite of spinel granulites from the Eastern Ghats Belt, India: evidence for polymetamorphism, a partial petrogenetic grid in the system KFMASH and the roles of ZnO and Fe_2O_3. J Petrol 36:435–461

Farver JR, Yund RA (1995) Volume and grain boundary diffusion of calcium in natural and hot-pressed calcite aggregates. Contrib Mineral Petrol 118:340–355

Fisher GW (1973) Nonequilibrium thermodynamics as a model for diffusion-controlled metamorphic processes. Am J Sci 273:897–924

Fisher GW (1978) Rate laws in metamorphism. Geochim Cosmochim Acta 42:1035–1050

Fisher GW, Elliott D (1974) Criteria for quasi-steady diffusion and local equilibrium in metamorphism. In: Hofmann AW et al (eds) Geochemical transport and kinetics. Carnegie Inst. Wash. Publ 634, pp 231–241

Holland TJB, Powell R (1998) An internally consistent thermodynamic data set for phases of petrological interest. J Metamorph Geol 16:309–343

Joesten R (1977) Evolution of mineral assemblage zoning in diffusion metasomatism. Geochim Cosmochim Acta 41:649–670

Joesten R (1991) Grain-boundary diffusion kinetics in silicate and oxide minerals. In: Ganguly J (ed) Diffusion, atomic ordering, and mass transport. Springer Berlin Heidelberg New York, pp 345–395

Kaur I, Mishin Y, Gust W (1995) Fundamentals of grain boundary and interphase boundary diffusion, 3rd edn. Wiley, Chichester

Keller LM, Abart R, Wirth R, Schmid DW, Kunze K (2006) Enhanced mass transfer through short-circuit diffusion: growth of garnet reaction rims at eclogite facies conditions. Am Mineral 91(7):1024–1038

Korzhinskii DS (1959) Physico-chemical basis of the analysis of the paragenesis of materials. Consultants Bureau, New York, 142 pp

Kretz R (1983) Symbols for rock forming minerals. Am Mineral 68:277–279

Lang HM, Wachter AJ, Peterson VL (2004) Coexisting clinopyroxene/spinel and amphibole/spinel symplectites in metatroctolites from the Buck Creek ultramafic body, North Carolina Blue Ridge. Am Mineral 89(1):20–30

Milke R, Heinrich W (2002) Diffusion-controlled growth of wollastonite rims between quartz and calcite: comparison between nature and experiment. J Metamorph Geol 20:467–480

Milke R, Wiedenbeck M, Heinrich W (2001) Grain boundary diffusion of Si, Mg, and O in enstatite reaction rims: a SIMS study using isotopically doped reactants. Contrib Mineral Petrol 142:15–26

Möller C (1998) Decompressed eclogites in the Sveconorwegian (–Grenvillian) orogen of SW Sweden: petrology and tectonic implications. J Metamorph Geol 20:641–656

Mongkoltip P, Ashworth JR (1983) Quantitative estimation of an open-system symplectite-forming reaction: restricted diffusion of Al and Si in coronas around olivine. J Petrol 24:635–661

Nakamura D (2002) Kinetics of decompressional reactions in eclogitic rocks—formation of plagioclase coronas around kyanite. J Metamorph Geol 20:325–333

Nakamura D, Hirajima T (2000) Granulite-facies overprinting of ultrahigh-pressure metamorphic rocks, northeastern Su–Lu region, eastern China. J Petrol 20:563–582

Newton RC, Charlu TV, Kleppa OJ (1980) Thermochemistry of high structural state plagioclases. Geochim Cosmochim Acta 44:933–941

Nichols GT, Berry RF, Green DH (1992) Internally consistent gahnitic spinel–cordierite–garnet equilibria in the FMASHZn system: geothermobarometry and applications. Contrib Mineral Petrol 111:362–377

Obata M (1994) Material transfer and local equilibria in a zoned kelyphite from a garnet pyroxenite, Ronda, Spain. J Petrol 35(1):271–287

O'Brien PJ (1999) Asymmetric zoning profiles in garnet from HP–HT granulite and implications for volume and grain-boundary diffusion. Mineral Mag 63(2):227–238

O'Brien PJ, Rötzler J (2003) High-pressure granulites: formation, recovery of peak conditions and implications for tectonics. J Metamorph Geol 21:3–20

Okay AI (1995) Paragonite eclogites from Dabie Shan, China: re-equilibration during exhumation? J Metamorph Geol 20:449–460

Powell R, Holland TJB (1999) Relating formulations of the thermodynamics of mineral solid solutions; activity modeling of pyroxenes, amphiboles and micas. Am Mineral 84(1–2):1–14

Schulmann K, Kröner A, Hegner E, Wendt I, Konopásek J, Lexa O, Štípská P (2005) Chronological constraints on the pre-orogenic history, burial and exhumation of deepseated rocks along the eastern margin of Variscan orogen, Bohemian Massif, Czech Republic. Am J Sci 305:407–448

Stüwe K (1997) Effective bulk composition changes due to cooling: a model predicting complexities in retrograde reaction textures. Contrib Mineral Petrol 129(1):43–52

Tajčmanová L, Konopásek J, Schulmann K (2006) Thermal evolution of the orogenic lower crust during exhumation within a thickened Moldanubian root of the Variscan belt of Central Europe. J Metamorph Geol 24:119–134

Thompson JB, Hovis GL (1979) Entropy of mixing in sanidine. Am Mineral 64:57–65

White RW, Powell R, Holland TJB (2001) Calculation of partial melting equilibria in the system Na_2O–CaO–K_2O–FeO–MgO–Al_2O_3–SiO_2–H_2O (NCKFMASH). J Metamorph Geol 19:139–153